Modelling [1 0 0] and [0 1 0] screw dislocations in MgSiO3 perovskite based on the Peierls-Nabarro-Galerkin model

Karine Gouriet, Philippe Carrez, Patrick Cordier

PAPER • OPEN ACCESS

Modelling [1 0 0] and [0 1 0] screw dislocations in MgSiO$_3$ perovskite based on the Peierls–Nabarro–Galerkin model

To cite this article: K Gouriet et al 2014 Modelling Simul. Mater. Sci. Eng. **22** 025020

View the article online for updates and enhancements.

Related content

- Dislocation modelling in Mg2SiO4 forsterite: an atomic-scale study based on the THB1 potential
  S Mahendran, P Carrez, S Groh et al.

- Peierls–Nabarro modelling of dislocation in MgO
  Philippe Carrez, Denise Ferré and Patrick Cordier

- Magnesium interatomic potential for simulating plasticity and fracture phenomena
  Z Wu, M F Francis and W A Curtin

Recent citations

- On the Origin of Radial Anisotropy Near Subducted Slabs in the Midmantle
  William Sturgeon et al

- The role of diffusion-driven pure climb creep on the rheology of bridgmanite under lower mantle conditions
  Riccardo Reali et al

- Dislocation modelling in Mg$_2$SiO$_4$ forsterite: an atomic-scale study based on the THB1 potential
  S Mahendran et al

Modelling [1 0 0] and [0 1 0] screw dislocations in MgSiO₃ perovskite based on the Peierls–Nabarro–Galerkin model

K Gouriet, Ph Carrez and P Cordier

Unité Matériaux et Transformation, CNRS UMR 8207, Université de Lille 1, Bât C6, 59655 Villeneuve d'Acsq, France

E-mail: philippe.carrez@univ-lille1.fr

Abstract

In this study, we model the core structure of screw dislocations with [1 0 0] and [0 1 0] Burgers vector in MgSiO₃ perovskite, in the pressure range of Earth's lower mantle (25–130 GPa). We use a generalized Peierls–Nabarro model, called Peierls–Nabarro–Galerkin, based on generalized stacking-fault energy calculations. These stacking-fault energy calculations are performed using a pairwise potential parametrization and compared to *ab initio* results. The results of Peierls–Nabarro–Galerkin calculations demonstrate that [1 0 0] dislocation and [0 1 0] are, respectively, characterized by a planar core spreading in (0 1 0) and (1 0 0). Our results emphasize the role of [1 0 0](0 1 0) and [0 1 0](1 0 0) slip systems in the deformation mechanism of MgSiO₃ perovskite. Furthermore, we validate the use of pairwise potential for further dislocation modelling of such minerals at the atomic scale.

Keywords: dislocations, MgSiO₃ perovskite, Peierls–Nabarro model

(Some figures may appear in colour only in the online journal)

S Online supplementary data available from stacks.iop.org/MSMSE/22/025020/mmedia

1. Introduction

Volcanism and earthquakes are spectacular manifestations of the internal activities of our planet that occur on a human timescale and that have a huge impact on mankind. Other geological

phenomena like mountain building and continental drift are only noticeable on geological timescales (billions of years). Since the 1960s, the study of plate tectonics has provided a general and coherent framework to rationalize most large-scale geological observations. A more global view is necessary, however, to understand the dynamics of the Earth. Our planet is still hot: 98% of its volume is at temperatures in excess of $1000\,°C$ and the total heat flux out of the Earth is estimated at about 44 TW. Transferring this heat through the mantle (made of thermally insulating rocks) can only be achieved by convection in the solid state. The lower mantle (between depths of about 670 km and 2900 km) is primarily constituted of a dense magnesium-rich silicate $((Mg,Fe,Al)(Si,Al)O_3)$ with a distorted perovskite structure. How this silicate creeps over geological times under mantle conditions is thus a major issue for geodynamics. In this study, we will focus on the magnesium end-member $(MgSiO_3)$ of this high-pressure phase (hereafter referred to as Mg-Pv).

The pressure range of the lower mantle (25–130 GPa) represents a major challenge to study the plastic behaviour of Mg-Pv under relevant mantle conditions. Consequently, very few experimental deformation studies have been performed on this phase (Merkel *et al* 2003, Cordier *et al* 2004, Wenk *et al* 2004, Miyajima *et al* 2009). Alternatively, recent studies have demonstrated that numerical multiscale modelling can provide complementary information on plasticity of high-pressure minerals under extreme conditions (Carrez *et al* 2007, Cordier *et al* 2012). Previous numerical models of dislocations in Mg-Pv were based on a one-dimensional Peierls–Nabarro (PN) model (1D-PN: Carrez *et al* 2007, Ferré *et al* 2007, Ferré *et al* 2009). Indeed, the PN model (Peierls 1940, Nabarro 1947) represents an elegant theoretical concept for modelling dislocation core structures that has heavily influenced dislocation theory. Its attractiveness has been reinforced with the development of atomistic calculations that allow us to calculate the (non-elastic) restoring forces in the core from generalized stacking-fault (GSF) calculations, also called γ-surface (see below). The PN model has therefore been applied to a large number of crystal structures, including minerals (Joos *et al* 1994, von Sydow *et al* 1999, Lu *et al* 2000, Lu 2005, Miranda and Scandolo 2005, Carrez *et al* 2006, Durinck *et al* 2007, Ferré *et al* 2008). However, it remains limited by some intrinsic assumptions (Schoeck 2005). In the 1D-PN model, only planar cores (in the glide plane) can be modelled, with possible dissociation restricted to collinear configurations. Hence, the GSF is calculated along the Burgers vector only (γ-lines). The drawback of these limitations is that the model potentially predicts different solutions for screw dislocations depending on the glide plane considered, since core spreading is forced to lie in this plane (see, e.g., figure 3 and table 3 in Ferré *et al* 2007). The Peierls–Nabarro–Galerkin (PNG) method (Denoual 2004, 2007) has been developed to overcome the limitations of the 1D-PN model. It is a generalization of the PN model for which non-collinear dissociations can be calculated by introducing two-dimensional GSFs (γ-surfaces) and non-planar cores can be modelled by taking into account several γ-surfaces simultaneously. Using this technique, it has been shown in MgO that $1/2\langle1\,1\,0\rangle$ screw dislocations in MgO change their glide planes with increasing pressure (Amodeo *et al* 2012).

The goal of this study is to take advantage of the new possibilities of the PNG model to re-investigate the structure of screw dislocations in $MgSiO_3$ perovskite. We focus on $[1\,0\,0]$ and $[0\,1\,0]$ dislocations that exhibit the lowest lattice friction on edge characters (Ferré *et al* 2007) and have already been characterized experimentally (Cordier *et al* 2004). We want to clarify the core structure of these screw dislocations (and hence their actual glide planes) at several pressures relevant for the Earth's lower mantle where the magnesium-rich silicate perovskite is stable. Due to the increased computational costs between γ-surfaces and γ-lines, atomistic calculations are performed here with an empirical potential (Oganov *et al* 2000). Since this empirical potential has never been used for calculating non-equilibrium (shear) configurations, a comparison with density functional theory (DFT) calculations is presented.

2. Computational methods

2.1. The Peierls–Nabarro–Galerkin method

In the PNG model, the dislocation core structure naturally emerges from the minimizing of an elastic energy and an interplanar potential. To illustrate the method, let us consider a unique slip plane Σ corresponding to a potential spreading plane of a dislocation core in a volume V. Continuous deformation around the dislocation core corresponds to a three-dimensional displacement field $u(r)$. In the same time, non-linear behaviour within the dislocation core can be represented by a two-dimensional displacement field $f(r)$, expressed in the normal basis of the Σ plane. Thus, the problem of core spreading consists of minimizing the energy E with respect to u and f according to equation (1), where Ω corresponds to the material density:

$$E = \int_V \left\{ E^{\mathrm{e}}[u, f] - \frac{1}{2}\Omega \dot{u}^2 \right\} \mathrm{d}V + \int_\Sigma E^{\mathrm{isf}}[f]\,\mathrm{d}\Sigma. \tag{1}$$

E^{e} corresponds to the elastic strain energy, whereas E^{isf} is the inelastic stacking-fault energy. The latter is a function of the γ-surface energies (to be defined in the next section) from which the linear elastic part has been subtracted. Finally, minimization with respect to f is achieved by means of a time-dependent Ginzburg–Landau equation, whereas an element-free Galerkin (Zienkiewicz and Taylor 2000) method is used to compute the evolution of $u(r)$. For the sake of clarity, the Galerkin method relies here on a two-dimensional nodal mesh (corresponding to mapping the x, y plane surrounding a dislocation aligned along the z axis). In doing so, the method allows us to also take into account several potential glide planes simultaneously and thus calculate complex (possibly three-dimensional) dislocation cores. Extended details of the PNG method are available in Denoual (2007), Pillon *et al* (2007) or Pillon and Denoual (2009).

The nodal meshes used in this study are built with respect to the *Pbnm* symmetry of Mg-Pv (Horiuchi *et al* 1987) considering the first four low index crystallographic planes to control the periodic variation of the dislocation core energy as a function of its position (see the online supplementary materials section, supplementary figure 1 stacks.iop.org/MSMSE/22/025020/mmedia). For all calculations, mesh dimensions are equivalent to 30 perovskite unit cells with a nodal resolution of 16 nodes per Burgers vector. Once nodes supporting γ-surface energies have been attributed, a discrete dislocation is introduced into the volume. Boundary conditions consistent with a dislocation in an infinite medium are used by imposing a convolution of an elementary elastic solution with the dislocation density (see Pillon and Denoual 2009 for implementation details). The equilibrium of displacement jump field f and the density of dislocation ρ, as defined as the derivative of f by the position coordinates, are finally determined through a viscous relaxation scheme. Accordingly to Denoual (2007), we check that increasing mesh dimensions or node numbers does not influence the results. The first calculations correspond to the relaxation of the dislocation core structure. In the second step, we evaluate the Peierls stress corresponding to the relaxed core. At this stage, a homogeneous deformation is progressively applied at a velocity that allows quasi-static equilibrium so as to induce an applied shear stress on a unique given glide plane. During this loading stage, noticeable evolution of the core structure may occur prior to a strong relaxation of the measured stress. Such relaxation of the measured stress is associated with a rapid evolution of the dislocation core structure followed by a displacement of one (or more) Burgers vectors. In the following, the Peierls stress will be associated to this ultimate macroscopic stress (Metsue *et al* 2010).

Table 1. Parametrization of pairwise potentials used (following Oganov *et al* 2000).

Bond ij	b_{ij} (eV)	ρ_{ij} (Å)	c_{ij} (eV.Å^6)
Mg–O	1041.435	0.2866	—
Si–O	1137.028	0.2827	—
O–O	2023.8	0.2674	13.83

2.2. Atomistic simulation details

Classical static simulations were performed using an interatomic pairwise potential (equation (2)) taking into account long-range and short-range interactions through Coulombic interactions and Buckingham forms, respectively. Short-range interactions include repulsive and attractive van der Waals interactions:

$$U_{ij}\left(r_{ij}\right) = \frac{z_i z_j}{r_{ij}} + b_{ij}\exp\left(-\frac{r_{ij}}{\rho_{ij}}\right) - \frac{c_{ij}}{r_{ij}^6}. \tag{2}$$

In equation (2), r_{ij} corresponds to the distance between ions of charge z_i; b_{ij}, ρ_{ij} and c_{ij} are constant parameters describing the short-range interactions. We use the parametrization proposed by Oganov *et al* (2000), known to be particularly robust for high-temperature and also high-pressure calculations (Oganov *et al* 2000, Liu *et al* 2007, Ito and Toriumi 2010, Chen *et al* 2012). This parametrization is described in table 1. Note that partial charges are used and cation–cation interactions are neglected at short range. Simulations have been performed using standard programming packages GULP (Gale 1997) and LAMMPS (Plimpton 1995). Both packages rely on Ewald summation methods (e.g. In't Veld *et al* 2007) for Coulombic interactions. Ground states properties of Mg-Pv (lattice parameter and elastic properties) were computed using GULP, whereas GSF energies were mostly determined with LAMMPS as discussed in the following section.

First principles calculations of γ-surface energies have also been performed within the framework of the DFT using the VASP package (Kresse and Hafner 1993, Kresse and Furthmüller 1996). Following the earlier work of Ferré *et al* (2007), we used the generalized gradient approximation (GGA) to model the exchange–correlation contributions (Perdew and Wang 1992) and ultrasoft pseudopotentials (e.g. Vanderbilt 1990 or Kresse and Hafner 1994) for ionic interactions. All calculations have been performed using a single cut-off energy value of 600 eV for the plane wave expansion and a Monkhorst–Pack grid (Monkhorst and Pack 1976) scheme was used for first Brillouin zone sampling.

2.3. Generalized stacking-fault energy calculations set-up

The generalized stacking-fault energy (i.e. γ-surface) represents the energy cost per unit area incurred by the relative shear displacement $\vec{f}$ across a plane of two perfect crystal halves. Atomistic calculations of the γ-surface generally involve the use of supercells and periodic boundary conditions. After shearing the supercell, atomic relaxations are allowed along the direction perpendicular to the fault plane exclusively.

For γ-surface calculations using DFT (VASP), we used the supercells from Ferré *et al* (2007). Due to calculation time limitations with DFT, the number of atomic layers parallel to the shear plane is limited and the supercell must terminate on a layer with fixed atoms followed by a vacuum buffer. In that case, the size of the supercell might not be sufficient to allow full relaxation of atomic positions close to the shear plane. To overcome this limitation, we have also performed γ-surface calculations using an empirical potential (LAMMPS). In that case,

Table 2. Athermal elastic constants and energy coefficient for screw dislocations of Burgers vectors [1 0 0] and [0 1 0]. Calculations of $K_{[100]}$ and $K_{[010]}$ are based on the elastic constant tensor (see the text for details).

Pressure (GPa)	30	60	100	140
a (Å)	4.65 (4.64)[a]	4.54	4.43 (4.37)[a]	4.34
b (Å)	4.76 (4.82)[a]	4.66	4.57 (4.62)[a]	4.49
c (Å)	6.72 (6.71)[a]	6.56	6.40 (6.37)[a]	6.28
C_{11}	620 (592)[a] (632)[b]	713 (753)[b]	818 (850)[a] (926)[b]	908
C_{22}	655 (672)[a] (735)[b]	771 (922)[b]	910 (1064)[a] (1160)[b]	1039
C_{33}	560 (617)[a] (653)[b]	688 (835)[b]	839 (997)[a] (1056)[b]	976
C_{44}	211 (235)[a] (250)[b]	237 (300)[b]	266 (334)[a] (360)[b]	291
C_{55}	215 (205)[a] (204)[b]	233 (234)[b]	252 (253)[a] (265)[b]	266
C_{66}	150 (192)[a] (212)[b]	183 (268)[b]	218 (306)[a] (330)[b]	250
C_{12}	235 (214)[a] (225)[b]	343 (320)[b]	484 (450)[a] (460)[b]	622
C_{13}	289 (197)[a] (209)[b]	369 (278)[b]	478 (382)[a] (380)[b]	587
C_{23}	285 (216)[a] (233)[b]	376 (306)[b]	486 (367)[a] (406)[b]	597
$K_{[1\,0\,0]}$	179 (197)[c]	206.34	234 (278)[c]	257
$K_{[0\,1\,0]}$	177 (212)[c]	208.17	241 (319)[c]	269

[a] DFT GGA calculations (Ferré *et al* 2007, Mainprice *et al* 2008).

[b] DFT LDA calculations (Wentzcovitch *et al* 1998).

[c] Dislocation energy coefficients based on DFT-GGA elastic constant tensor.

we use fully periodic supercells built on lattice parameters (a_1, a_2, a_3). The supercells involve a repetition of at least eight perovskite unit cells along the normal to the slip plane. a_1 and a_2 correspond to the shortest crystallographic lattice vectors parallel to the γ-surface. When stacking faults are introduced by displacing the upper block with respect to the lower one, the lattice vector a_3 is tilted along $\vec{f}$ to keep periodicity. Energy minimization is then undertaken, keeping volume constant. This procedure has been followed for the (1 0 0), (0 1 0) and (0 0 1) γ-surfaces. The drawback is that this procedure can only be applied to γ-surfaces for which a_3 is aligned with a crystallographic axis. For a *Pbnm* orthorhombic structure, some γ surfaces involving shear in (1 0 1) or (0 1 1) do not meet this requirement. For (1 0 1) γ-surfaces, it is possible to use the high-index crystallographic axis [25 0 12] as an approximation of the normal direction (with a departure of 1° from the true normal orientation). It is worth noting that it may induce some distortions compared to a perfect bulk system. For (0 1 1) γ-surfaces, keeping reasonably low distortions was not possible. We therefore used the same kind of supercells as for DFT calculations with a vacuum buffer along the direction normal to the shear plane. However, size is not a limitation and we used a neutral supercell containing at least 3280 atoms.

3. Results

An orthorhombic $MgSiO_3$ perovskite unit cell (containing 20 atoms, i.e. 4 formula unit) is first fully optimized at 30, 60, 100 and 140 GPa through static calculations performed with the GULP package. Regarding the elastic properties, the full athermal elastic constant tensors were derived from stress–strain relations (Barron and Klein 1965, Wallace 1972) implemented in GULP. As expected from the potential parametrizations used (Oganov *et al* 2000), the bulk properties (table 2) are found in good agreement with the available literature data, including
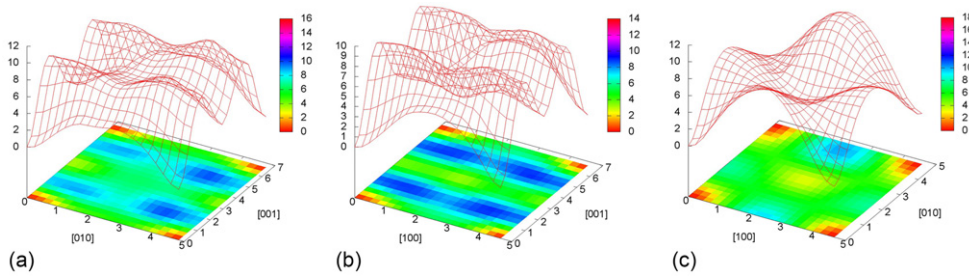
Figure 1. γ-surface ($\mathrm{J\,m^{-2}}$) landscapes calculated at 30 GPa using VASP code (see the text for details). (*a*) (1 0 0), (*b*) (0 1 0) and (*c*) (0 0 1).

the DFT calculations. Only C_{33} and C_{66} are slightly softer and C_{13} and C_{23} are stiffer. As a consequence, the energy coefficient for screw dislocations of Burgers vectors [1 0 0] and [0 1 0], calculated within the framework of the Stroh theory using the DisDi software (Douin *et al* 1986), are found to be lower in case of pairwise potential calculations and also less anisotropic compared to DFT-based evaluations.

3.1. γ-surfaces

Static calculations using LAMMPS and the pairwise potentials have been performed for five types of γ-surfaces at four pressures, i.e. γ-surfaces corresponding to (1 0 0), (0 1 0), (0 0 1), (0 1 1) and (1 0 1) planes at 30, 60, 100 and 140 GPa. DFT calculations have only be performed for the (1 0 0), (0 1 0) and (0 0 1) planes at 30 and 100 GPa. This was motivated by comparison purposes and validity arguments of pairwise potential calculations.

Figure 1 shows (1 0 0), (0 1 0) and (0 0 1) γ-surfaces calculated at 30 GPa using VASP. Due to the symmetry elements of the *Pbnm* space group, each γ-surface exhibits a mirror plane. The mirror is perpendicular to [0 0 1] in (1 0 0) and (0 1 0) and to [1 0 0] in (0 0 1). Mirrors are associated with γ-surface extrema (metastable or unstable stacking-fault energies). Along [0 0 1], we find a 1/2[0 0 1] stable stacking fault in (1 0 0) and (0 1 0). For the three γ-surfaces, the lowest energy paths are systematically found along [1 0 0] or [0 1 0] with an asymmetric profile along [0 1 0] in (1 0 0) and (0 0 1) and along [1 0 0] in (0 1 0). Increasing pressure to 100 GPa leads to a severe increase of γ-surface energies, with the lowest energy paths being multiplied by 1.5–2 (figure 2).

Figure 3 shows the results of pairwise potential calculations for the five γ-surfaces (only those calculated at 140 GPa are presented). The agreement with the DFT calculations is shown in figure 2 along some γ-lines. Not only the shape (including asymmetries) but also the energies involved are well captured using the pairwise potential. Whatever the γ-surface (and applied pressure), the largest energy differences between the two calculations types correspond to unstable fault configurations (with an energy difference smaller than $3\,\mathrm{J\,m^{-2}}$), whereas in case of stable faults, the energy differences are reduced below $1\,\mathrm{J\,m^{-2}}$. The pairwise potential parametrization is thus able to reproduce the asymmetry of energy profiles as well as their evolutions with pressure. Finally, for (1 0 1) and (0 1 1) planes (figures 3(*d*) and (*e*)), stable stacking faults are present at the centre of the γ-surface. Regarding the influence of pressure, as already mentioned for the DFT calculations, increasing pressure induces an increase of γ-surface energies (see the online supplementary materials section, supplementary figures 3, 4 and 5 stacks.iop.org/MSMSE/22/025020/mmedia).
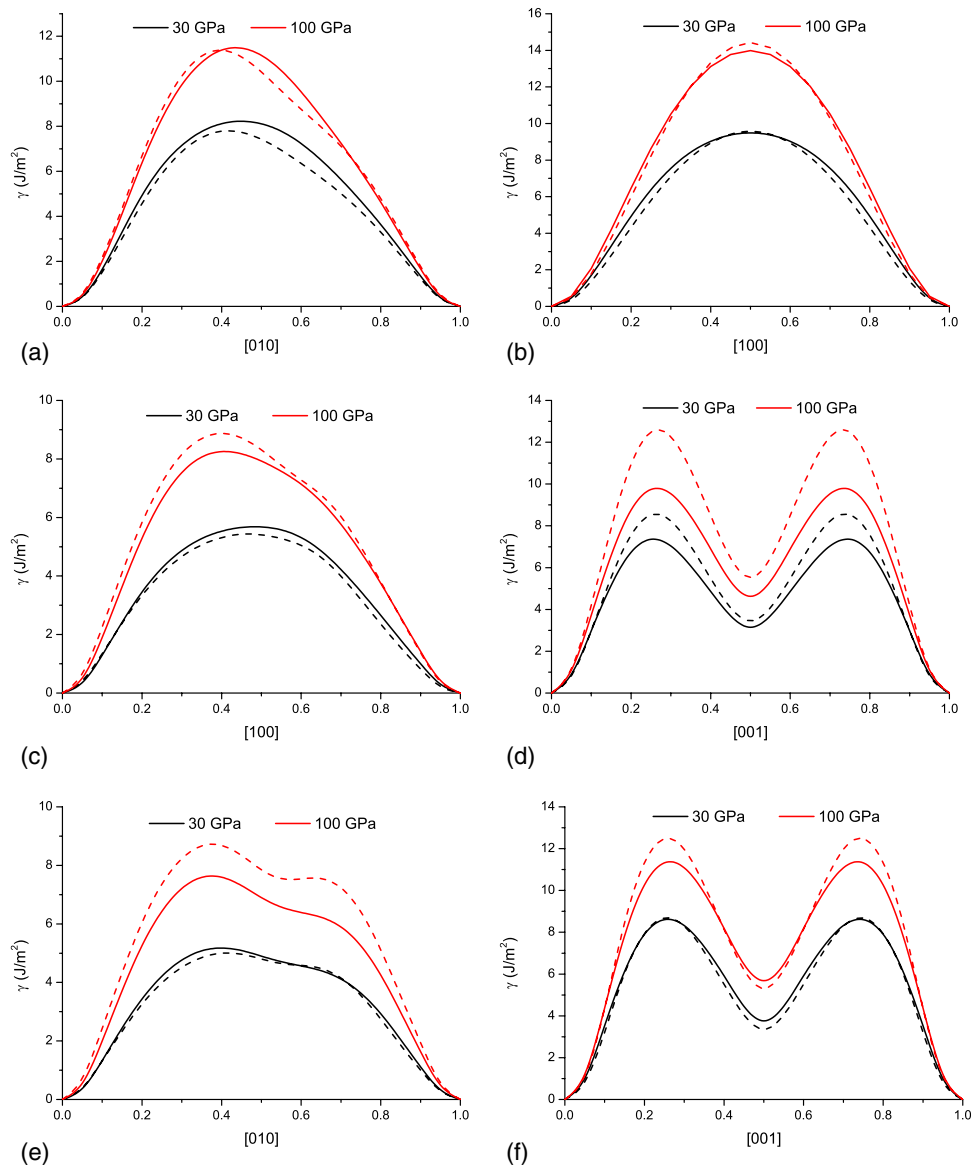
Figure 2. Comparison between pairwise potential calculations (straight line) and DFT results (dotted lines) for a selection of γ-lines. γ-lines along [0 1 0] (*a*) and [1 0 0] (*b*) in (0 0 1), along [1 0 0] (*c*) and along [0 0 1] (*d*) in (0 1 0), along [0 1 0] (*e*) and [0 0 1] (*f*) in (1 0 0). For comparison, γ-lines are plotted as a function of normalized shear vectors.

3.2. Dislocation core structures

Dislocation core structures are calculated with the PNG method. As an input of the PNG model, we used γ-surfaces calculated with pairwise potentials with the LAMMPS package, and elasticity tensors determined with the GULP package.
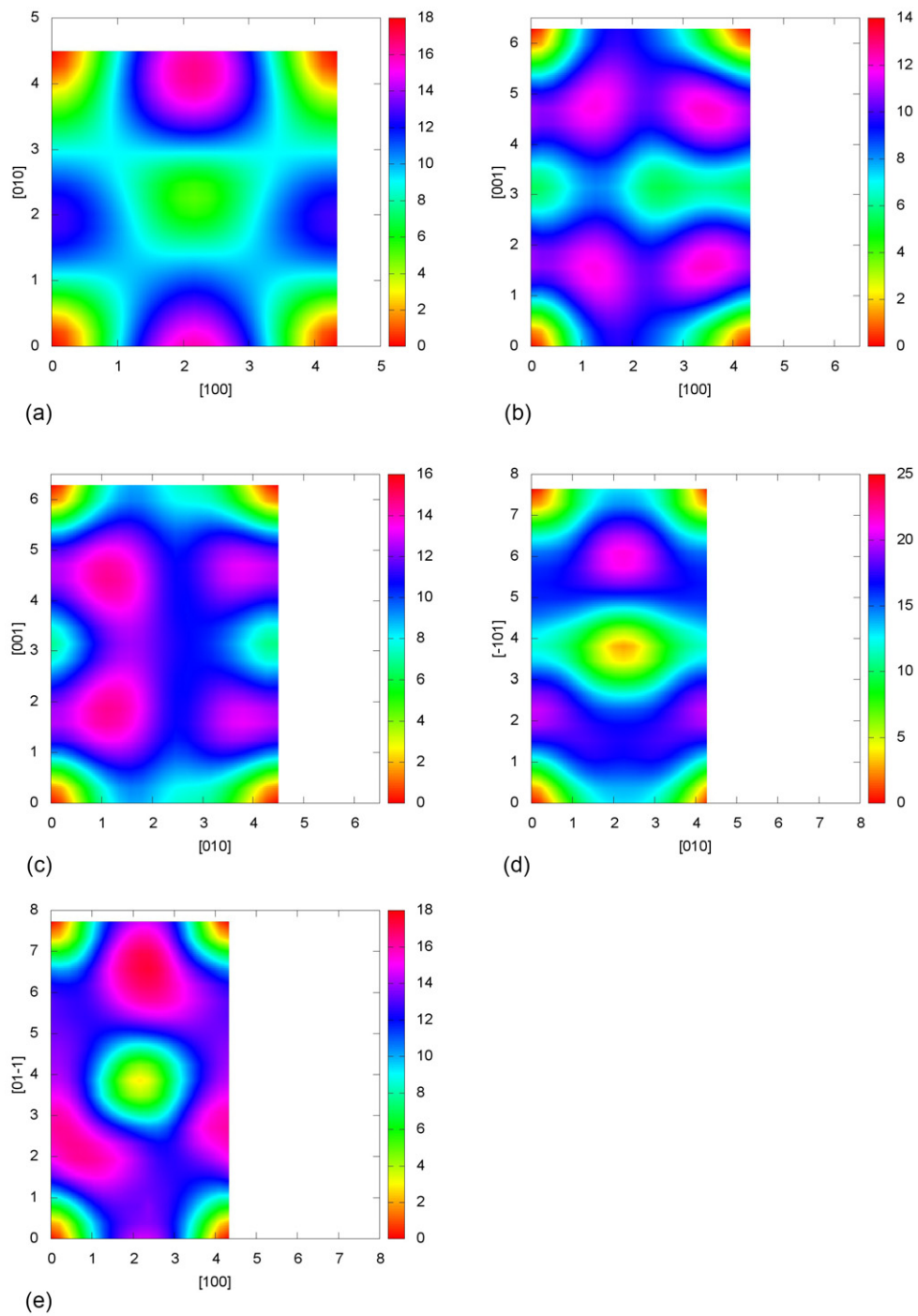
Figure 3. Contour plot of γ-surfaces $(J\,m^{-2})$ calculated at $140\,GPa$ using pairwise potentials. (*a*) (0 0 1), (*b*) (0 1 0), (*c*) (1 0 0), (*d*) (1 0 1) and (*e*) (0 1 1).
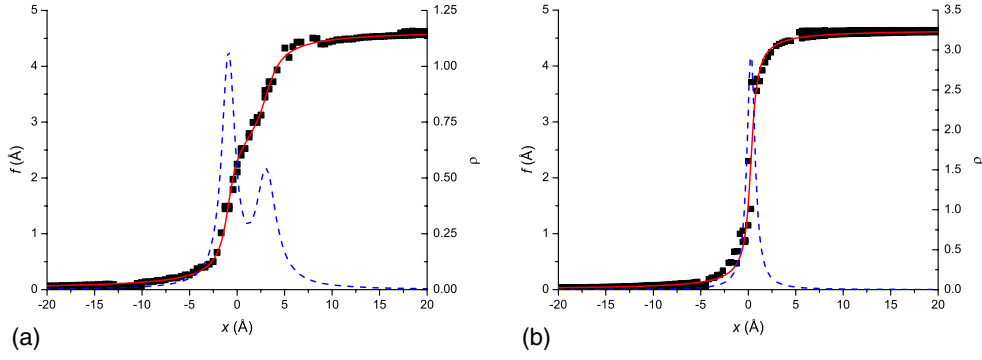
Figure 4. Core structure of the [1 0 0] screw dislocation calculated with an applied pressure of 30 GPa. Disregistry function $f(x)$ and associated Burgers vector density $\rho = \mathrm{d}f(x)/\mathrm{d}x$ (dotted line) are plotted in (0 1 0) (*a*) and (0 0 1) (*b*) planes.
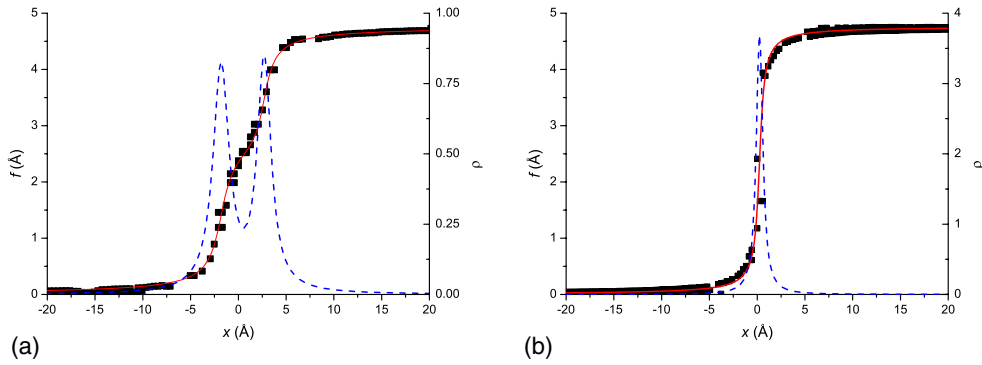
Figure 5. Core structure of the [0 1 0] screw dislocation calculated with an applied pressure of 30 GPa. Disregistry function $f(x)$ and associated Burgers vector density $\rho = \mathrm{d}f(x)/\mathrm{d}x$ (dotted line) are plotted in (1 0 0) (*a*) and (0 0 1) (*b*) planes.

3.2.1. [0 0 1] and [0 1 0] screw dislocation cores at 30 GPa. For the [1 0 0] screw dislocation, we introduce the four crystallographic planes (0 1 0), (0 0 1), (0 1 1) and (0 1 $\bar{1}$) containing [1 0 0] (the Burgers vector) through the corresponding γ-surfaces in the PNG model. Analysis of node displacement resulting from the relaxation of the dislocation core shows no edge component. Screw displacements are mostly in the (0 1 0) and (0 0 1) planes. To represent the core structure, we focus on the disregistry f (parallel to the Burgers vector) by plotting the nodes disregistries as a function of the distance from the core in (0 1 0) and (1 0 0) (figure 4). Similarly, to model the screw dislocation with the [0 1 0] Burgers vector, we used the (1 0 0), (0 0 1), (1 0 1) and (1 0 $\bar{1}$) planes. As for the [1 0 0] screw dislocation, the [0 1 0] dislocation remains of pure screw character with the largest node displacements in the (1 0 0) and (0 0 1) planes (figure 5). Note that both core structures exhibit a narrow core in (0 0 1) and a wider spreading in (0 1 0) or (1 0 0) (for the [1 0 0] and [0 1 0] Burgers vectors, respectively). This tendency for core spreading is indicated by a shoulder on the disregistry curve. As such a feature may indicate a tendency for dissociation, we performed a smooth fitting of the disregistry functions using a sum of arctan functions (equation (3)), whereas for the (0 0 1) plane, we rely on the canonical analytical solution (i.e. $i = 0$ and $x_i = 0$ in equation (3) of Peierls 1940)

$$f(x) = \frac{b}{2} + \frac{b}{\pi} \sum_i \alpha_i \arctan\left(\frac{x - x_i}{\zeta_i}\right). \tag{3}$$

9

Table 3. [1 0 0] screw dislocation core parameters controlling the spreading in the (0 1 0) and (0 0 1) planes. Half-widths are given in Angstroms (also in reduced coordinate ζ/a' in brackets where a' is taken as the lattice distance in the direction of spreading). The separation distance Δ between the two fractionals in (0 1 0) is expressed in Angstroms.

| Pressure (GPa) | (0 1 0) | | | | | (0 0 1) |
| | 1st fractional | | 2nd fractional | | | |
	α_1	ζ_1	α_2	ζ_2	Δ	ζ
30	0.57	0.80 (0.12)	0.43	1.25 (0.19)	3.97	0.48 (0.10)
60	0.56	0.74 (0.11)	0.44	1.17 (0.18)	3.88	0.45 (0.10)
100	0.55	0.61 (0.10)	0.45	1.03 (0.16)	3.58	0.40 (0.09)
140	0.70	0.67 (0.11)	0.30	0.82 (0.13)	3.11	0.54 (0.12)

Table 4. Same as table 3 for [0 1 0] screw dislocation cores spread in the (1 0 0) and (0 0 1) planes.

| Pressure (GPa) | (1 0 0) | | | | | (0 0 1) |
| | 1st fractional | | 2nd fractional | | | |
	α_1	ζ_1	α_2	ζ_2	Δ	ζ
30	0.47	0.85 (0.13)	0.53	0.99 (0.15)	4.51	0.39 (0.08)
60	0.45	0.95 (0.14)	0.55	0.73 (0.11)	3.89	0.55 (0.12)
100	0.41	0.57 (0.09)	0.59	0.83 (0.13)	3.78	0.41 (0.09)
140	0.24	0.34 (0.05)	0.76	0.89 (0.14)	2.98	0.54 (0.13)

The parameters describing the calculated relaxed cores are given in tables 3 and 4. The misfit distribution can be described as two asymmetrical fractional dislocations separated by a distance Δ (corresponding to $x_1 - x_2$ in equation (3)). In case of the [1 0 0] dislocation, the separation width between the two fractionals is slightly lower than 4 Å, however, the fractionals remain strongly correlated due to the width ζ_i of fractionals being greater than 1 Å. For the [0 1 0] screw dislocation, the tendency toward dissociation is more pronounced with two almost identical fractional peaks and a separation width of 4.5 Å.

3.2.2. Evolution of dislocation cores with pressure and Peierls stress calculations. For calculations performed under pressures above 30 GPa, the main characteristics of the dislocation cores remain unchanged, i.e. we still find fractional decomposition of the [1 0 0] screw dislocation in (0 1 0) and of the [0 1 0] screw dislocation in (1 0 0). At the same time, core spreading in (0 0 1) remains very limited with a reduced half-width (ζ/a', where a' is the lattice distance in the spreading direction) around 0.1 (tables 3 and 4). Core calculations performed at 30, 60, 100 and 140 GPa are presented in figure 6. Increasing pressure induces a noticeable decrease of the fractional width separation (at 140 GPa, fractionals of [0 1 0] dislocation are separated by less than 3 Å compared to the initial separation distance of 4.5 Å at 30 GPa).

As mentioned in section 2.1, the Peierls stresses (σ_p) for the four slip systems investigated here, [1 0 0](0 1 0), [1 0 0](0 0 1), [0 1 0](1 0 0) and [0 1 0](0 0 1), have been evaluated by shearing the PNG nodal mesh. For each slip system, we applied positive or negative shear component. We observe distinct behaviours with respect to the sign of the applied stress. A typical example of core modification prior to displacement is given in figure 7. Therefore, we define here two Peierls stresses for each slip system (summarized in table 5). The difference
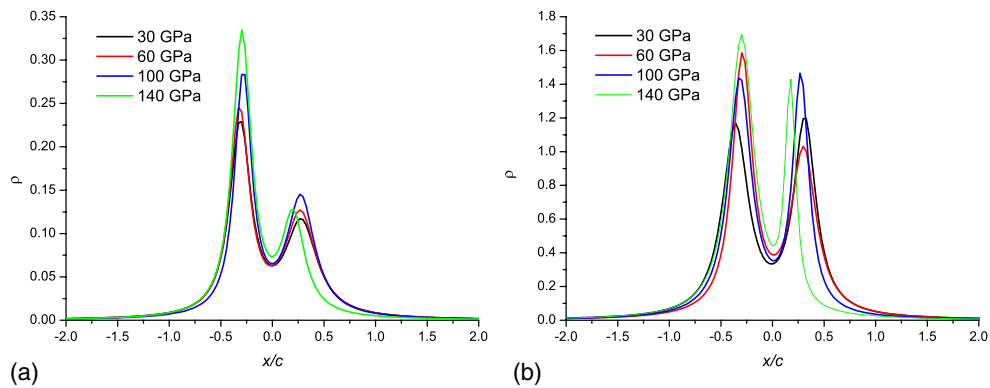
Figure 6. Evolution of Burgers vector density ρ as a function of pressure. (*a*) Core spreading of a [1 0 0] dislocation in (0 1 0). (*b*) Core spreading of a [0 1 0] dislocation in (1 0 0). Distance x from the core is normalized to the length c of the lattice direction [0 0 1].

between positive and negative Peierls stresses can be substantial, with largest discrepancies found in (0 0 1). Nevertheless, whatever the pressure or the direction of the applied strain, stresses required to move [1 0 0] and [0 1 0] dislocations in the (0 1 0) and (1 0 0) planes, respectively, are always found to be significantly lower than the stresses for glide in (0 0 1).

4. Discussion

Dislocation core calculations generally imply a cluster or dipole method to determine atomistic arrangement within the core (see, e.g., Woodward 2005 or Vitek and Paidar 2008). Such calculations are largely developed in material science and used for core structure calculations in metal or semiconductors (Yamaguchi and Vitek 1973, Xu and Moriarty 1998, Woodward and Rao 2002, Wang *et al* 2003, Pizzagalli and Beauchamp 2004, Ventelon and Willaime 2007, Groger *et al* 2008, Clouet 2009, Pizzagalli *et al* 2009, Proville *et al* 2012). However, for minerals and more generally ionic compounds, the number of studies is still limited (Woo and Puls 1977, Watson *et al* 1999, Walker *et al* 2004, 2005, Hirel *et al* 2012). A main reason is related to the technical difficulty in tracting large-scale simulations on material already containing tens of atoms in a unit cell and more than two atomic species (Walker *et al* 2010). Atomistic calculations of dislocation core structures in minerals or ceramics therefore rely on the use of empirical potentials. In such a context, the present study suggests that pairwise potential can be used for atomistic calculations of dislocation cores in Mg-Pv.

The first point of comparison is between γ-surface calculations based on pairwise potential and DFT calculations. Whatever the pressure investigated, we find that pairwise potential calculations are able to capture the energy landscape (shape and energy level) of γ-surfaces calculated with DFT. In particular, the non-symmetric shape of γ-surfaces (figures 1 and 3) attributed to the tilting of octahedra in orthorhombic Mg-Pv (Ferré *et al* 2007, 2009) is well reproduced by the pairwise potentials. The most significant discrepancies come from the maximum unstable energies along the [0 0 1] shear directions in the (1 0 0) and (0 1 0) planes (figure 2). DFT maximum energies are indeed higher without actually showing large discrepancies for the stable stacking energies at 1/2[0 0 1]. We believe that this can be attributed to a size effect of the DFT simulation cells. Indeed, the supercells used for the DFT calculations
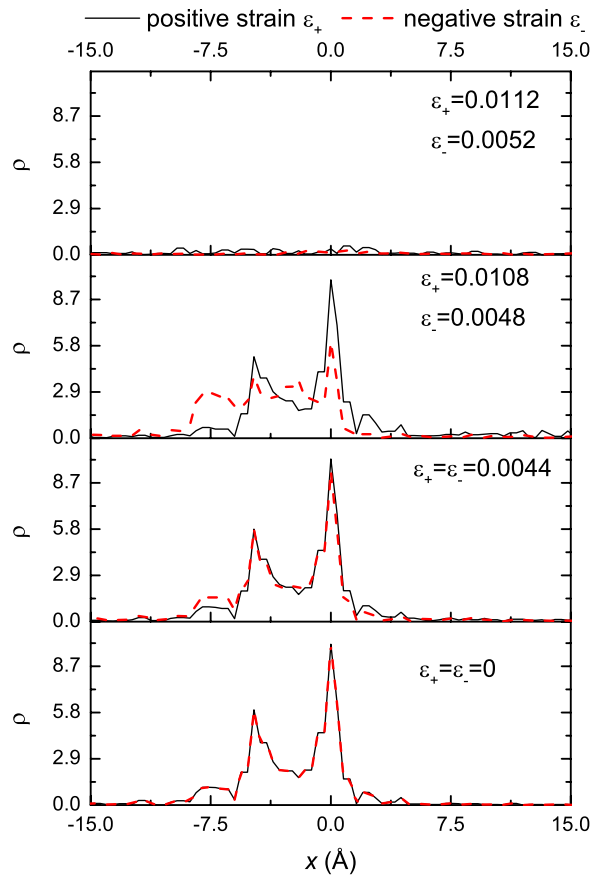
Figure 7. Illustration of the non-symmetric behaviour of [0 1 0] dislocations submitted to an applied positive or negative strain to induce glide in ($\bar{1}$ 0 0). In this example, a negative applied strain induces a first modification of the lowest fractional, which starts to move for $\varepsilon_- = 0.0048$. It is then followed by a rapid evolution of the whole core structure with an irreversible displacement at $\varepsilon_- = 0.0052$. On the contrary, for an applied positive strain, the largest fractional seems to be stable up to $\varepsilon_+ = 0.0108$, prior to the whole displacement of the core at 0.0112.

correspond to two unit cells (40 atoms) only, including frozen atoms on supercell surfaces. This leaves less than a half unit cell to accommodate the imposed shear and relax the energy. Such supercell geometry is thus expected to overestimate unstable configuration energies. In the same time, stable stacking-fault configurations appear less sensitive to the degree of freedom allowed with a better agreement between the DFT and pairwise potential calculations. Therefore it seems that the parametrization of pairwise potentials used here is demonstrated to be able to reproduce the shear properties of the Mg-Pv structure under large strains beyond the classic elasticity limits used by Oganov *et al* (2000) to fit the potentials.

The second critical point to examine is the dislocation core structures. The cores of the [1 0 0] screw dislocations (table 3) are mostly spread in (0 1 0), similarly the cores of the [0 1 0] dislocations (table 4) are spread in ($\bar{1}$ 0 0). Both cores tend to display planar spreading. Analysis of node displacements never indicates the formation of any edge component, suggesting a purely collinear decomposition into fractional dislocations. This is

Table 5. Peierls stresses (σ_p in GPa). The two values correspond to the ultimate stress prior to dislocation irreversible displacement for a positive (and negative, respectively) applied shear strain.

Pressure (GPa)	[1 0 0](0 1 0)	[1 0 0](0 0 1)	[0 1 0](1 0 0)	[0 1 0](0 0 1)
30	0.4–0.2	5.1–4.3	0.2–1.0	12.2–7.2
60	1.9–1.6	7.5–6.1	2.5–1.2	13.3–6.9
100	1.2–2.1	12.6–8.6	1.3–0.3	17.8–8.2
140	2.3–1.5	10.6–6.9	1.5–3.6	17.1–10.0

clearly a consequence of the γ-surfaces landscapes, for which no stable configuration close to the [1 0 0] or [0 1 0] directions exist in (1 0 0) or (0 1 0), respectively. Another consequence of γ-surface energies is the fact that dislocation cores tend to spread in a plane characterized by the lowest GSF energy. Due to the non-symmetric shape of γ-lines in these planes, core structures are thus non-symmetric. The core structures of the dislocations in (1 0 0) and (0 1 0) are consistent with a previous determination of core spreading based on the DFT results and 1D-PN modelling (Ferré *et al* 2007, see also the online supplementary figures 7–10 stacks.iop.org/MSMSE/22/025020/mmedia). In other words, in case of a planar dislocation core with a tendency of collinear dissociation, both the PNG approach and the 1D-PN model lead to similar results. However, the limitations of the 1D-PN model are evidenced by the comparison of core spreading in (0 0 1). Based on an intrinsic assumption of the planar core, the 1D-PN model predicts a wider core for both screw dislocations in (0 0 1) (see the online supplementary figures 7–10). One achievement of the PNG model is thus to determine the core spreading of dislocations without any ambiguities. As a consequence, the easiest slip systems should be [1 0 0](0 1 0) and [0 1 0](1 0 0), confirmed by the order of magnitude of difference of Peierls stresses for glide of the same dislocations in (0 0 1) (table 5). It is worth noting that these two slip systems are also suggested by the few experimental studies of plastic deformation of Mg-Pv under Earth's mantle pressure conditions (Karato *et al* 1990, Chen *et al* 2002, Merkel *et al* 2003, Cordier *et al* 2004). More generally, [1 0 0](0 1 0) and [0 1 0](1 0 0) can be related (assuming a relationship between the distorted structure and the ideal cubic one) to the most common slip systems ⟨1 1 0⟩{1 1 0} in cubic perovskite (Nishigaki *et al* 1991, Matsunaga and Saka 2000, Brunner *et al* 2001, Gumbsch *et al* 2001). Nevertheless, while ⟨1 1 0⟩ dislocations are dissociated into well-separated partial dislocations in cubic perovskite (Carrez *et al* 2010, Hirel *et al* 2012), [1 0 0] and [0 1 0] dislocations are not strictly identical with no pronounced dissociation schemes. These can be interpreted in terms of the distortions of the orthorhombic Mg-Pv structure (Ferré *et al* 2009), also responsible for the non-symmetric energy landscape of the γ-surfaces. Another interesting feature related to the distortions of the structure (and non-symmetric γ-surfaces) is the non-identical behaviours of dislocations under a positive or negative applied strain (figure 7). Depending of the sign of the applied strain (or stress), two Peierls stresses can be identified. The ratio between the positive and negative σ_p can be greater than two and specially marked for [0 1 0](0 0 1). Differential behaviours of dislocation cores with respect to applied stress are commonly reported in bcc metals (see Wang *et al* 2003 for instance) and attributed to twinning/anti-twinning mechanisms. To our knowledge, it is the first evidence of such anomalies in a perovskite. In previous studies (Ferré *et al* 2007, Mainprice *et al* 2008, Ferré *et al* 2009), the Peierls stress was defined as the maximum slope of misfit energy (equation (3) of Ferré *et al* 2007 for instance, corresponding to a discrete summation of γ-surface energies accordingly to the dislocation disregistry) without focusing on the misfit energy variation details. Consequently, for relevant
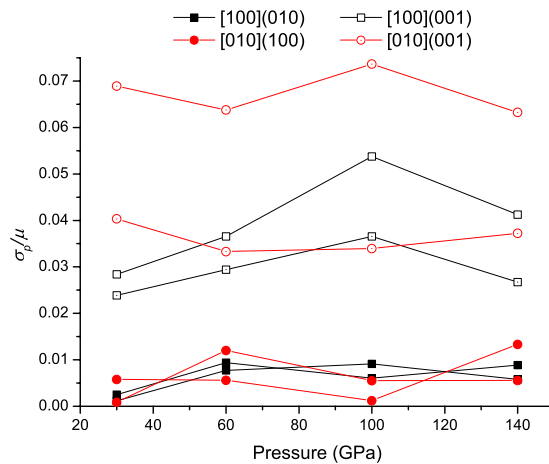
Figure 8. Evolution of the Peierls stresses σ_p (normalized to the shear modulus μ) as a function of pressure for the four slip systems investigated. For each slip system, two Peierls stresses are reported, corresponding to the dislocation behaviour submitted to positive or negative strain (see the text for details).

comparison with previous σ_p evaluations, we should only focus here on the highest Peierls stress values (table 5). Strong disparities between the 1D-PN and PNG models are obvious with current PNG calculations being significantly lower than the results from 1D-PN modelling (discrepancies can reach two orders of magnitude). If we take elasticity variations (between DFT and pairwise potential modelling) into account through the energy coefficient K (K replaces the isotropic shear modulus μ, see Hirth and Lothe 1982), normalized stresses (figure 8) evolve between 10^{-3}–10^{-2} μ for [1 0 0](0 1 0) and [0 1 0](1 0 0), and 2×10^{-2}–8×10^{-2} μ for [1 0 0](0 0 1) and [0 1 0](0 0 1). Again, the PNG calculations are one order of magnitude lower than previous 1D-PN results (see Ferré *et al* 2009). As discussed by Schoeck (2005), the observed discrepancies could be the consequence of the 1D-model assumptions. In particular, differentiating the Peierls stress from the misfit energy does not account for possible core modifications under stress and, accordingly, variation of the elastic energy. The PNG model accounts for both core modifications and elastic energy variations. It is also worth noticing that accurate Peierls stress calculation remains a challenging issue and may require strong refinement, as shown in a recent study by Proville *et al* (2012). At this stage, it is therefore preferable to consider the differences between Peierls stresses of different slip systems calculated within the same model. Here, this highlights the importance of the [1 0 0](0 1 0) and [0 1 0](1 0 0) slip systems in Mg-Pv within the pressure range of Earth mantle.

Regarding the core behaviour under stress, the stress (or strain) threshold for dislocation displacement seems to be related to the dissociation into distinct fractionals. The lowest Peierls stress value systematically corresponds to the first displacement of the widest fractional, whereas the highest value is reached when the dislocation displacement involves the first modification of the narrowest fractional (figure 7). Further investigation of this mechanism is, however, difficult to achieve by PNG as a whole displacement of the core occurs very rapidly after the first event. Therefore, further atomistic calculations are mandatory to understand this phenomenon. We believe that atomistic calculations based on the pairwise potential parametrization used here could help clarify these observations.

5. Concluding remarks

Based on the generalized PN model, this study clarifies the core structure of screw dislocations of Burgers vectors [1 0 0] and [0 1 0] in magnesium silicate perovskite (Mg-Pv) in a pressure range of 30–140 GPa. Screw cores are found to spread in (0 1 0) and (1 0 0), suggesting the major role of the [1 0 0](0 1 0) and [0 1 0](1 0 0) slip systems in this orthorhombic perovskite structure. In contrast to previous studies (Ferré *et al* 2007, Mainprice *et al* 2008, Ferré *et al* 2009), current calculations rely on an empirical parametrization of pairwise potentials (Oganov *et al* 2000). We show that the pairwise potentials calculations of γ-surface energies compare well with the DFT calculations. The accuracy of the pairwise potentials to model non-equilibrium configurations, especially the large atomistic displacements involved in dislocation cores, opens a new route to full atomistic calculations of the dislocations and mechanical properties in Mg-Pv.

Acknowledgments

References

Amodeo J, Carrez Ph and Cordier P 2012 Modelling the effect of pressure on the critical shear stress of MgO single crystals *Phil. Mag.* **92** 1523–41

Barron T H K and Klein M L 1965 Second-order elastic constants of a solid under stress *Proc. Phys. Soc. Lond.* **85** 523–32

Brunner D, Taeri-Baghbadrani S, Sigle W and Ruhle M 2001 Surprising results of a study on the plasticity in strontium titanate *J. Am. Ceram. Soc.* **84** 1161–3

Carrez Ph, Cordier P, Mainprice D and Tommasi A 2006 Slip systems and plastic shear anisotropy in Mg_2SiO_4 ringwoodite: insights from numerical modelling *Eur. J. Mineral.* **18** 149–60

Carrez Ph, Ferré D and Cordier P 2007 Peierls–Nabarro model for dislocations in $MgSiO_3$ post-perovskite calculated at 120 GPa from first principles *Phil. Mag.* **87** 3229–47

Carrez Ph, Ferré D, Denoual C and Cordier P 2010 Modelling thermal activation of $\langle 1\,1\,0 \rangle \{1\,1\,0\}$ slip at low temperature in $SrTiO_3$ *Scr. Mater.* **63** 434–7

Chen J H, Weldner D J and Vaughan M T 2002 The strength of $Mg_{0.9}Fe_{0.1}SiO_3$ perovskite at high pressure and temperature *Nature* **419** 824–6

Chen Y, Chernatynskiy A, Brown D, Schelling P K, Artacho E and Phillpot S R 2012 Critical assessment of classical potentials for $MgSiO_3$ perovskite with application to thermal conductivity calculations *Phys. Earth Planet. Interiors* **210** 75–89

Clouet E 2009 Elastic energy of a straight dislocation and contribution from core tractions *Phil. Mag.* **89** 1565–84

Cordier P, Amodeo J and Carrez Ph 2012 Modelling the rheology of MgO under Earth's mantle pressure, temperature and strain rates *Nature* **481** 177–80

Cordier P, Ungar T, Zsoldos L and Tichy G 2004 Dislocation creep in $MgSiO_3$ perovskite at conditions of the Earth's uppermost lower mantle *Nature* **428** 837–40

Denoual C 2004 Dynamic dislocation modeling by combining Peierls–Nabarro and Galerkin methods *Phys. Rev. B* **70** 024106

Denoual C 2007 Modeling dislocation by coupling Peierls–Nabarro and element-free Galerkin methods *Comput. Methods Appl. Mech. Eng.* **196** 1915–23

Douin J, Veyssiere P and Beauchamp P 1986 Dislocation line stability in Ni_3Al *Phil. Mag.* A **54** 375–93

Durinck J, Carrez Ph and Cordier P 2007 Application of the Peierls–Nabarro model to dislocations in forsterite *Eur. J. Mineral.* **19** 631–9

Ferré D, Carrez Ph and Cordier P 2007 First principles determination of dislocations properties of $MgSiO_3$ perovskite at 30 GPa based on the Peierls–Nabarro model *Phys. Earth Planet. Interiors* **163** 283–91

Ferré D, Carrez Ph and Cordier P 2008 Modeling dislocation cores in $SrTiO_3$ using the Peierls–Nabarro model *Phys. Rev.* B **77** 014106

Ferré D, Carrez Ph and Cordier P 2009 Peierls dislocation modelling in perovskite ($CaTiO_3$): comparison with tausonite ($SrTiO_3$) and $MgSiO_3$ perovskite *Phys. Chem. Min.* **36** 233–9

Gale J D 1997 GULP: A computer program for the symmetry-adapted simulation of solids *J. Chem. Soc. Faraday Trans.* **93** 629–37

Groger R, Bailey A G and Vitek V 2008 Multiscale modeling of plastic deformation of molybdenum and tungsten: I. Atomistic studies of the core structure and glide of $1/2\langle 1\,1\,1\rangle$ screw dislocations at 0 K *Acta Mater.* **56** 5401–11

Gumbsch P, Taeri-Baghbadrani S, Brunner D, Sigle W and Ruhle A 2001 Plasticity and an inverse brittle-to-ductile transition in strontium titanate *Phys. Rev. Lett.* **87** 085505

Hirel P, Mrovec M and Elsasser C 2012 Atomistic simulation study of $\langle 1\,1\,0\rangle$ dislocations in strontium titanate *Acta Mater.* **60** 329–38

Hirth J and Lothe J 1982 *Theory of Dislocations* (New York: Wiley)

Horiuchi H, Ito E and Weidner D J 1987 Perovskite-type $MgSiO_3$—single crystal x-ray–diffractions study *Am. Mineralogist* **72** 357–60

In't Veld P J, Ismail A E and Grest G S 2007 Application of Ewald summations to long-range dispersion forces *J. Chem. Phys.* **127** 144711

Ito Y and Toriumi M 2010 Silicon self-diffusion of $MgSiO_3$ perovskite by molecular dynamics and its implication for lower mantle rheology *J. Geophys. Res.—Solid Earth* **115** B12205

Joos B, Ren Q and Duesbery M S 1994 Peierls–Nabarro model of dislocations in silicon with generalized stacking-fault restoring forces *Phys. Rev.* B **50** 5890–8

Karato S, Fujino K and Ito E 1990 Plasticity of MgSiO3 perovskite—the results of microhardness tests on single-crystals *Geophys. Res. Lett.* **17** 13–16

Kresse G and Furthmuller J 1996 Efficient iterative schemes for ab initio total-energy calculations using a plane-wave basis set *Phys. Rev.* B **54** 11169–86

Kresse G and Hafner J 1993 Ab-initio molecular-dynamics for liquid-metals *Phys. Rev.* B **47** 558–61

Kresse G and Hafner J 1994 Ab-initio molecular-dynamics simulation of the liquid-metal amorphous-semiconductor transition in germanium *Phys. Rev.* B **49** 14251–69

Liu Z J, Sun X W, Tan X M, Guo Y D and Yang X D 2007 Structural and thermodynamic properties of $MgSiO_3$ perovskite under high pressure and high temperature *Solid State Commun.* **144** 264–8

Lu G 2005 The Peierls–Nabarro model of dislocations: a venerable theory and its current development *Handbook of Materials Modeling* ed S Yip (Dordrecht: Springer)

Lu G, Kioussis N, Bulatov V V and Kaxiras E 2000 The Peierls–Nabarro model revisited *Phil. Mag. Lett.* **80** 675–82

Mainprice D, Tommasi A, Ferré D, Carrez Ph and Cordier P 2008 Predicted glide systems and crystal preferred orientations of polycrystalline silicate Mg-Perovskite at high pressure: implications for the seismic anisotropy in the lower mantle *Earth Planet. Sci. Lett.* **271** 135–44

Matsunaga T and Saka H 2000 Transmission electron microscopy of dislocations in $SrTiO_3$ *Phil. Mag. Lett.* **80** 597–604

Merkel S, Wenk H R, Badro J, Montagnac G, Gillet P, Mao H K and Hemley R J 2003 Deformation of ($Mg_{0.9}$, $Fe_{0.1}$)SiO_3 Perovskite aggregates up to 32 GPa *Earth Planet. Sci. Lett.* **209** 351–60

Metsue A, Carrez Ph, Denoual C, Mainprice D and Cordier P 2010 Plastic deformation of wadsleyite: IV dislocation core modelling based on the Peierls–Nabarro–Galerkin model *Acta Mater.* **58** 1467–78

Miranda C R and Scandolo S 2005 Computational materials science meets geophysics: dislocations and slip planes of MgO *Comput. Phys. Commun.* **169** 24–7

Miyajima N, Yagi T and Ichihara M 2009 Dislocation microstructures of $MgSiO_3$ perovskite at a high pressure and temperature condition *Phys. Earth Planet. Interiors* **174** 153–58

Monkhorst H J and Pack J D 1976 Special points for Brillouin-zone integrations *Phys. Rev.* B **13** 5188–92

Nabarro F R N 1947 Dislocations in a simple cubic lattice *Proc. Phys. Soc. Lond.* **59** 256–72

Nishigaki J, Kuroda K and Saka H 1991 Electron-microscopy of dislocation-structures in $SrTiO_3$ deformed at high-temperatures *Phys. Status Solidi* a—*Appl. Res.* **128** 319–36

Oganov A R, Brodholt J P and Price G D 2000 Comparative study of quasiharmonic lattice dynamics, molecular dynamics and Debye model applied to $MgSiO_3$ perovskite *Phys. Earth Planet. Interiors* **122** 277–88

Peierls R 1940 The size of a dislocation *Proc. Phys. Soc.* **52** 34–7

Perdew J P and Wang Y 1992 Accurate and simple analytic representation of the electron-gas correlation-energy *Phys. Rev.* B **45** 13244–9

Pillon L and Denoual C 2009 Inertial and retardation effects for dislocation interactions *Phil. Mag.* **89** 127–41

Pillon L, Denoual C and Pellegrini Y P 2007 Equation of motion for dislocations with inertial effects *Phys. Rev.* B **76** 224105

Pizzagalli L and Beauchamp P 2004 First principles determination of the Peierls stress of the shuffle screw dislocation in silicon *Phil. Mag. Lett.* **84** 729–36

Pizzagalli L, Demenet J L and Rabier J 2009 Theoretical study of pressure effect on the dislocation core properties in semiconductors *Phys. Rev.* B **79** 045203

Plimpton S 1995 Fast parallel algorithms for short-range molecular-dynamics *J. Comput. Phys.* **117** 1–19

Proville L, Rodney D and Marinica M C 2012 Quantum effect on thermally activated glide of dislocations *Nature Mater.* **11** 845–9

Schoeck G 2005 The Peierls model: progress and limitations *Mater. Sci. Eng.* A **400** 7–17

Vanderbilt D 1990 Soft self-consistent pseudopotentials in a generalized eigenvalue formalism *Phys. Rev.* B **41** 7892–5

Ventelon L and Willaime F 2007 Core structure and Peierls potential of screw dislocations in alpha-Fe from first principles: cluster versus dipole approaches *J. Comput.-Aided Mater. Des.* **14** 85–94

Vitek V and Paidar V 2008 Non-planar dislocation cores: a ubiquitous phenomenon affecting mechanical properties of crystalline materials *Dislocations in Solids* ed H John (Amsterdam: Elsevier) chapter 87

von Sydow B, Hartford J and Wahnstrom G 1999 Atomistic simulations and Peierls–Nabarro analysis of the Shockley partial dislocations in palladium *Comput. Mater. Sci.* **15** 367–79

Walker A M, Carrez Ph and Cordier P 2010 Atomic-scale models of dislocation cores in minerals: progress and prospects *Min. Mag.* **74** 381–413

Walker A M, Gale J D, Slater B and Wright K 2005 Atomic scale modelling of the cores of dislocations in complex materials: I. Methodology *Phys. Chem. Chem. Phys.* **7** 3227–34

Walker A M, Slater B, Gale J D and Wright K 2004 Predicting the structure of screw dislocations in nanoporous materials *Nature Mater.* **3** 715–20

Wallace D C 1972 *Thermodynamics of Crystals* (New York: Wiley)

Wang G F, Strachan A, Cagin T and Goddard W A 2003 Role of core polarization curvature of screw dislocations in determining the Peierls stress in bcc Ta: a criterion for designing high-performance materials *Phys. Rev.* B **67** 224101

Watson G W, Kelsey E T and Parker S C 1999 Atomistic simulation of screw dislocations in rock salt structured materials *Phil. Mag.* A **79** 527–36

Wenk H R, Lonardelli I, Pehl J, Devine J, Prakapenka V, Shen G and Mao H K 2004 *In situ* observation of texture development in olivine, ringwoodite, magnesiowustite and silicate perovskite at high pressure *Earth Planet. Sci. Lett.* **226** 507–19

Wentzcovitch R M, Karki B B, Karato S and Da Silva C R S 1998 High pressure elastic anisotropy of MgSiO$_3$ perovskite and geophysical implications *Earth Planet. Sci. Lett.* **164** 371–8

Woo C H and Puls M P 1977 Atomistic breathing shell-model calculations of dislocation core configurations in ionic-crystals *Phil. Mag.* **35** 727–56

Woodward C 2005 First-principles simulations of dislocation cores *Mater. Sci. Eng.* A **400** 59–67

Woodward C and Rao S I 2002 Flexible *ab initio* boundary conditions: Simulating isolated dislocations in bcc Mo and Ta *Phys. Rev. Lett.* **88** 216402

Xu W and Moriarty J A 1998 Accurate atomistic simulations of the Peierls barrier and kink-pair formation energy for ⟨1 1 1⟩ screw dislocations in bcc Mo *Comput. Mater. Sci.* **9** 348–56

Yamaguchi M and Vitek V 1973 Core structure of nonscrew 1/2⟨1 1 1⟩ dislocations on {1 1 0} planes in BCC crystals: I. Core structure in an unstressed crystal *J. Phys. F: Met. Phys.* **3** 523–36

Zienkiewicz O C and Taylor R L 2000 *The Finite Element Method* (Oxford: Butterworth-Heinemann)